

Rethinking Seismic Source Model of Probabilistic Hazard Assessment in Taiwan after the 2018 Hualien, Taiwan, Earthquake Sequence

by Chung-Han Chan, Kuo-Fong Ma, Ya-Ting Lee, and Yu-Ju Wang

ABSTRACT

We examined the performance of Taiwan earthquake model (TEM) PSHA2015. We retrospectively forecasted the seismic activities of the 2018 Hualien, Taiwan, sequence and proposed recommendations for the next generation of seismic hazard assessment for Taiwan. We confirmed the model credibility of the area sources by comparing with locations of the Hualien sequence and seismicity during the period from 2012 to 2016. We also concluded similar forecasting reliability for the smoothing model, which could be incorporated in the next generation of probabilistic seismic-hazard analysis (PSHA) as a branch of logic tree. To examine the performance of the seismogenic structure source model, we evaluated rupture probability of the Milun fault, which ruptured during the Hualien sequence. The TEM PSHA2015 model forecasts its rupture probability in 50 yrs as 53%, and the Brownian passage time (BPT) model forecasts 80%. The BPT model, considering also time-dependency rupture probability, is suggested for future hazard assessment, especially for the seismogenic structure sources with records of their last ruptures. This earthquake sequence has raised the importance of short-term seismic hazard assessment, which provides a basis for response after a devastating earthquake and/or forecasting consequence.

INTRODUCTION

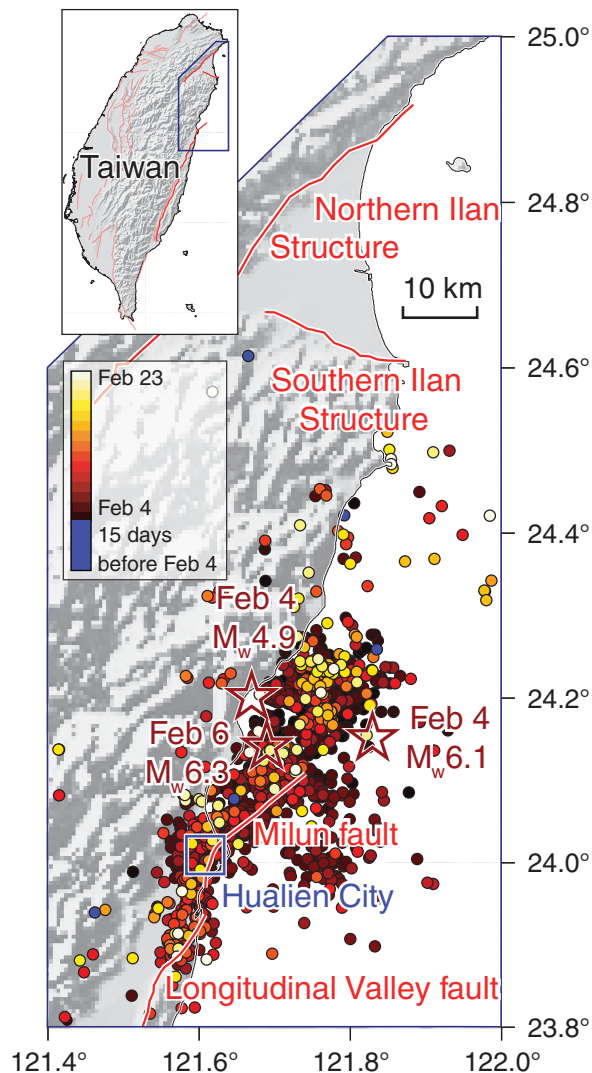
When a M_w 4.9 earthquake rattled the east coast of Taiwan on 4 February, people did not pay much attention until another M_w 6.1 event took place within an hour (Fig. 1). Because these events were far from a populated area, no damage was reported. Two days after the initiation of this sequence, on 6 February, another larger earthquake of M_w 6.3 took place close to Hualien City, a scenic city with a population of more than 100,000 that also attracts many visitors. This earthquake, unfortunately, resulted in damage and fatality, including some international travelers (Wu *et al.*, 2018). During this event, surface rupture along the Milun fault was observed. After occurrence of this sequence, the awareness of seismic hazard mitigation in this

region increased and probabilistic seismic hazard analysis (PSHA) is one of the practical approaches for this purpose (Cornell, 1968).

The Taiwan earthquake model (TEM) team has constructed the most recent hazard model for Taiwan (as known as TEM PSHA2015; Wang, Chan, *et al.*, 2016). This model includes two categories of crustal seismic sources, that is, shallow-background area and seismogenic structure sources. In this model, the geometry of each shallow-background area source is defined subjectively (Cheng *et al.*, 2015), and the seismicity rate is assumed to be uniform in each individual source. Alternatively, Chan *et al.* (2012) proposed a seismic model for Taiwan using the smoothing approach by Woo (1996), which does not require subjectively definition of zonation. Besides, the seismicity model of the TEM PSHA2015 is time independent; that is, previous earthquakes do not trigger consequent ones and active faults do not contain memory time elapse of last rupture. Such assumption, however, has been questioned since earthquakes are dependent in both time and space (e.g., Harris, 1998). Thus, Chan *et al.* (2017) proposed a time-dependent PSHA for the Taiwan region, considering long- and short-term time-dependent factors through the Brownian passage time (BPT; Ellsworth *et al.*, 1999) and the rate-and-state friction law (Dieterich, 1994), respectively.

Because several PSHAs have been proposed, their performance credibility should be validated. Although Wang, Lee, *et al.* (2016) evaluated the TEM PSHA2015 model in terms of strong ground shaking, their seismicity rate models for the seismogenic sources have not yet been discussed. The 2018 Hualien sequence could be an ideal case to validate the PSHA performance due to the large magnitude of the mainshock and complexity of spatial and temporal distribution.

Thus, in this study, we retrospectively forecast the earthquake distribution using the models of the TEM PSHA2015 and Chan *et al.* (2012, 2017). We will first compare the performance of the shallow-background area source and smoothing model. Then different rupture models for seismogenic structure sources will be validated. In addition, we will raise



▲ **Figure 1.** Distribution of the 2018 Hualien sequence and neighboring seismicogenic structure sources. The three largest events in this sequence are denoted as red stars. Hualien City is denoted as blue rectangle. Occurrence date of each event in the sequence is denoted in color.

the importance of time dependency on PSHA. Based on our forecast results, we will propose some suggestions for future hazard assessment.

PERFORMANCE OF THE TEM MODEL IN LONG-TERM SEISMICITY ACTIVITY

The TEM PSHA2015 model, in addition to the subduction zone sources, includes two source types for crustal events: shallow-background area and seismicogenic structure sources. We will validate their performance of earthquake forecasting and compare with other models from various PSHAs.

Performance of the Shallow-Background Area Source

The TEM PSHA2015 defines 28 shallow-background area sources to illustrate seismicity activity with focal depths shallower than 30 km.

The seismicity rate for each source is represented as a - and b -values of the Gutenberg–Richter relationship (Gutenberg and Richter, 1944) according to the best-fit regression with complete part of earthquake catalog (i.e., $M_w \geq 4.0$ for 1973–1992 and $M_w \geq 3.0$ for 1993–2011). We converted number of events (in the form of a - and b -values) of each source into seismicity density (in/km²/yr) considering their coverage area (Table 1). In comparison, the three largest events in the Hualien sequence (red stars in Fig. 2) are in the areas with high-seismic densities; that is, the M_w 4.9 and 6.1 events (stars 1 and 2, respectively) are in the area S15, with the highest seismic density (3.98×10^{-3} events/km²/yr) among the 28 shallow-background area source; the M_w 6.3 event is in the area S17A (3.10×10^{-3} events/km²/yr), the third highest density region that follows S16 (3.68×10^{-3} events/km²/yr), confirming good forecasting ability of the background-shallow area source model for moderate earthquakes.

To further validate the performance of the TEM PSHA2015 in a long-term period, we forecasted the earthquakes during the period from 2012 to 2016. The earthquake parameters are accessed from the database of the Central Weather Bureau Seismic Network. Most of the events take place along the eastern coastline and offshore in the northeast (open circles in Fig. 2), confirming feasibility of the TEM PSHA2015 model. To quantify the forecasting ability, the correlation between the model and observations was assessed through the Molchan diagram (Molchan, 1990, and references therein).

This diagram evaluates forecasting ability through presenting the alarm-occupied space as a function of failure fraction in forecasting, considering the locations of the observations with respect to the distribution of modeled seismicity density. The “fraction of alarm-occupied space” is the percentage of observations within the region with a forecasting level equal to or higher than “alarm”; the “fraction of failure in forecasting” is the percentage of observations having a lower forecasting level than the alarm. That is, when data points distribute along a diagonal line, the distribution of observations is independent of model; convex distribution suggests that the majority of observations occur within regions with a lower forecasted rate, whereas concavity suggests that the majority of observations are within high-forecasted rate areas.

To implement the TEM PSHA2015 model into the Molchan diagram, we identified the corresponding area for each 0.05° by 0.05° cell in the study area (shown in Fig. 2) and read its seismicity density in this model (from Table 1) to compare with distribution of the forecasting events (circles in Fig. 2a). Because the TEM PSHA2015 model illustrates seismicity activity for $M_w \geq 4.0$, we compared the distribution of earthquakes with the same magnitude threshold (shown in Fig. 3a). To test its forecasting ability for large events that might result in seismic hazard, we also implemented the distribution of earthquakes with $M_w \geq 6.0$ (shown in Fig. 3b). The data points generally show concavity distribution for both cases of $M_w \geq 4.0$ and $M_w \geq 6.0$, confirming the forecasting ability of the TEM PSHA2015 model. Furthermore, the null hypothesis (Zechar and Jordan, 2008) shows a 99% signifi-

Table 1
***a*- and *b*-Values, Size of the Area, Corresponding Density for $M_w \geq 4.0$ Seismicity Obtained by Taiwan Earthquake Model (TEM) PSHA2015; Rate Change after 4 February and after 6 February Obtained by the Rate-And-State Friction Model**

Area	<i>a</i> -Value	<i>b</i> -Value	Size (km)	Area	Density ($M_w \geq 4$)	Rate Change after 4 February (%)	Rate Change after 6 February (%)
S01	3.69	1.07	37,289	S01	6.89×10^{-6}	0.5	3.5
S02	4.01	1.07	16,356	S02	3.28×10^{-5}	0.0	0.8
S03	3.66	1.07	14,025	S03	1.71×10^{-5}	0.0	0.0
S04	3.17	1.07	4,277	S04	1.81×10^{-5}	1.9	11.4
S05A	3.57	1.07	2,656	S05A	7.34×10^{-5}	3.6	16.8
S05B	4.32	1.07	1,917	S05B	5.72×10^{-4}	3.8	12.7
S06	4.63	1.07	3,402	S06	6.58×10^{-4}	1.1	10.7
S07	4.72	1.07	3,817	S07	7.21×10^{-4}	0.0	0.7
S08A	4.14	1.07	4,316	S08A	1.68×10^{-4}	0.0	0.2
S08B	3.74	1.07	6,991	S08B	4.12×10^{-5}	0.0	0.2
S09	3.98	1.07	1,589	S09	3.15×10^{-4}	13.8	171.3
S10	4.80	1.07	1,879	S10	1.76×10^{-3}	4.6	107.9
S11	4.63	1.07	2,892	S11	7.74×10^{-4}	0.3	2.4
S12	4.84	1.07	5,969	S12	6.08×10^{-4}	0.0	0.4
S13	4.37	1.07	8,706	S13	1.41×10^{-4}	0.7	2.3
S14A	4.34	1.07	1,616	S14A	7.10×10^{-4}	41.4	463.2
S14B	4.92	1.07	3,207	S14B	1.36×10^{-3}	6.1	21.4
S14C	4.79	1.07	4,626	S14C	6.99×10^{-4}	4.1	9.4
S15	5.33	1.07	2,819	S15	3.98×10^{-3}	27,303.0	2,394.4
S16	5.56	1.07	5,178	S16	3.68×10^{-3}	4.8	22.2
S17A	5.21	1.07	2,740	S17A	3.10×10^{-3}	55.5	846.1
S17B	4.42	1.07	1,407	S17B	9.80×10^{-4}	66.2	122.3
S18A	4.91	1.07	2,806	S18A	1.52×10^{-3}	0.7	7.0
S18B	4.58	1.07	2,205	S18B	9.04×10^{-4}	0.3	8.6
S19A	5.16	1.07	3,551	S19A	2.13×10^{-3}	0.0	0.9
S19B	4.60	1.07	2,786	S19B	7.49×10^{-4}	0.0	1.1
S20	4.53	1.07	14,624	S20	1.22×10^{-4}	0.0	0.2
S21	5.12	1.07	28,197	S21	2.45×10^{-4}	2.1	8.8

cance level for the model based on the number of the observations (603 earthquakes), suggesting the 99% confidence level that cannot reject this model (because all of the blue circles are below the gray ones in Fig. 3).

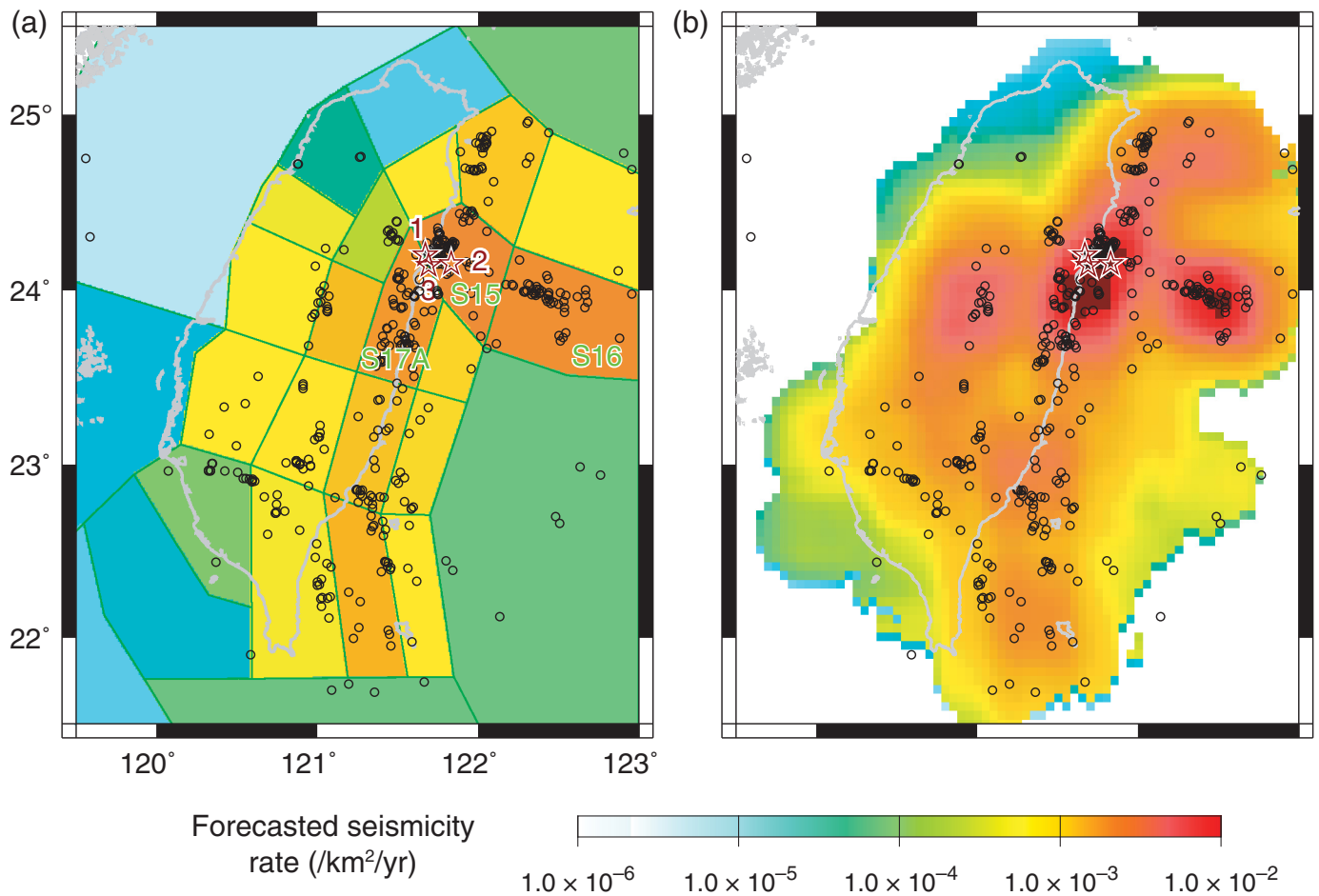
The foregoing analyses confirmed the forecasting ability of the TEM PSHA2015 model. Because this model is constructed based on past seismicity activity, other time-independent models based on the same catalog might provide good forecasts as well. Thus, we proposed another forecasting model based on the smoothing approach of Woo (1996), which does not require subjective definition of area source. This approach summarizes past seismicity activity based on the smoothing kernel as a function of the magnitude M and the distance between the site of interest and the epicenter of the i th earthquake $x - x_i$, represented as follows:

$$K(M, x - x_i) = \frac{PL - 1}{\pi H^2(M)} \left(1 + \left(\frac{x - x_i}{H(M)} \right)^2 \right)^{-PL}, \quad (1)$$

in which PL denotes the power law index. The bandwidth function $H(M)$ is defined as the mean distance between each event with magnitude M and its nearest neighbour, represented as follows:

$$H(M) = c \times e^{d \times M}, \quad (2)$$

in which c and d are constants that can be obtained by regression. Following the procedure of Chan *et al.* (2012), we implemented the same earthquake catalog as the TEM PSHA2015 (i.e., $M_w \geq 4.0$ earthquakes for 1973–1992 and $M_w \geq 3.0$ earthquakes for 1993–2011) and determined that the c and d values of the bandwidth function are 0.0187 and 1.1156, respectively, to model the seismicity density for the Taiwan region (Fig. 2b). In comparing with the area source model (Fig. 2a), the smoothing model does not include density discontinuity. Except such discrepancy, both models forecast high-seismic density along the eastern coastline and offshore in the



▲ **Figure 2.** Seismicity density model by (a) Taiwan earthquake model (TEM) PSHA2015 and (b) the smoothing approach of Woo (1996). Open circles denote earthquakes with $M_w \geq 4.0$ during 2012 and 2016. Stars 1–3 denote 4 February M_w 4.9, 4 February M_w 6.1, and 6 February M_w 6.3 earthquakes, respectively.

northeast, consistent with observations during 2012 and 2016 (open circles in Fig. 2). The forecasting ability is further confirmed through Molchan diagrams that all data points locate on the lower left corner of the diagrams and pass the null hypothesis (because all green circles are below the gray ones in Fig. 3). In comparing the two models, both forecast well for the $M_w \geq 4.0$ events (Fig. 3a), whereas the shallow-background area source model of the TEM PSHA2015 forecasts better in the $M_w \geq 6.0$ case for 3.6 percentiles (Fig. 3b).

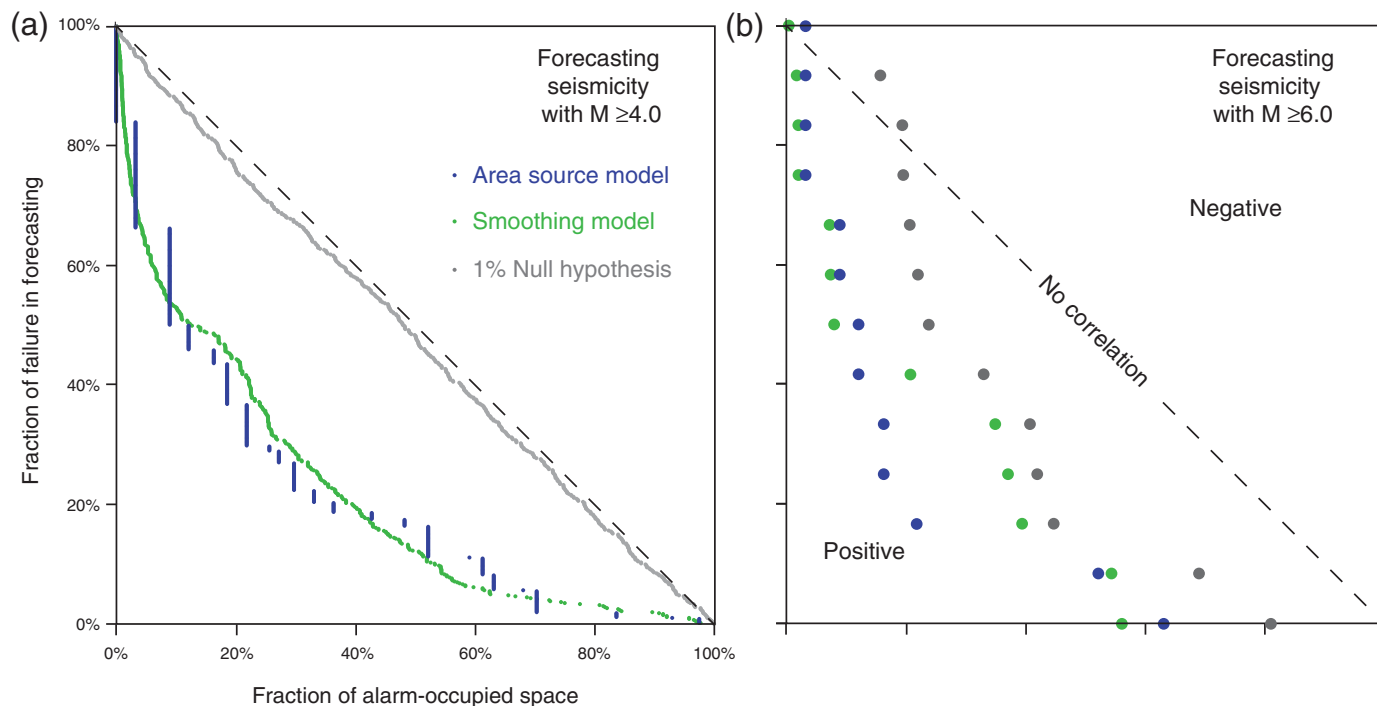
Performance of the Seismogenic Structure Source

The credibility of the shallow-background area source model of the TEM PSHA2015 has been proven above. The performance of other crustal seismic sources in the TEM PSHA2015, seismogenic structure sources, can also be validated through the Hualien sequence because the 6 February M_w 6.3 event results in rupture of the Milun fault, one of the seismogenic structure sources in this model (Yen *et al.*, 2018).

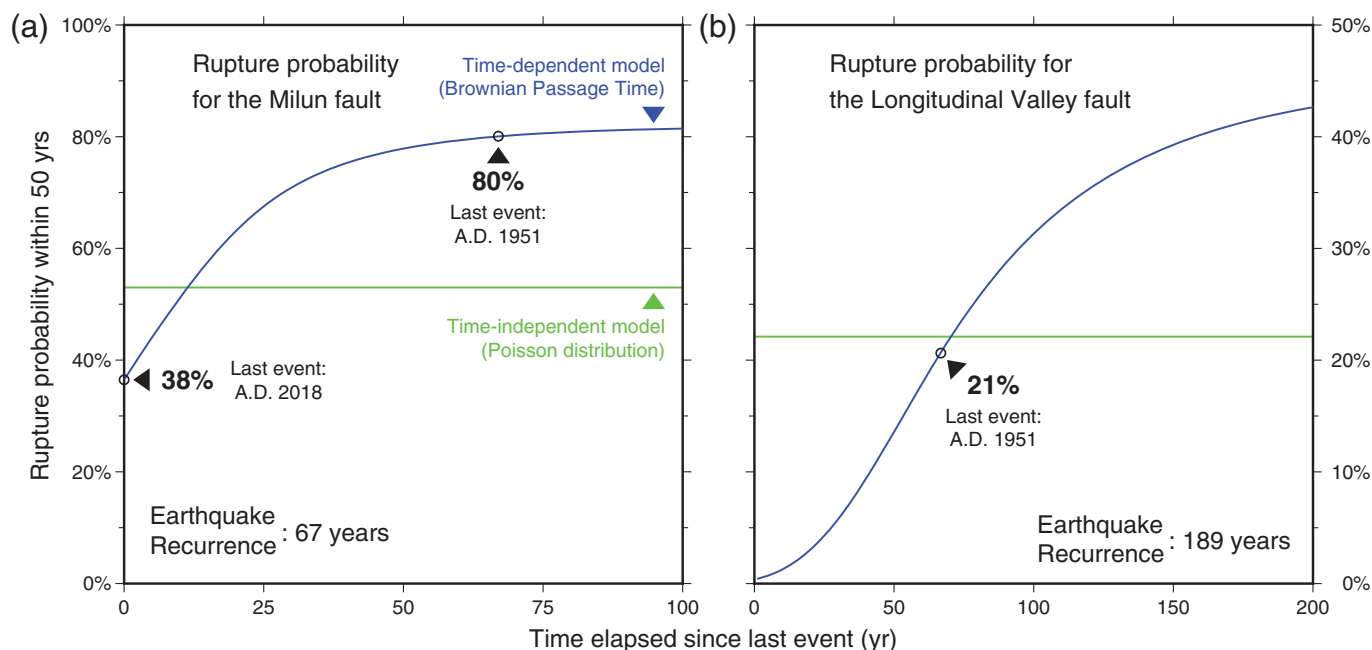
In the TEM seismogenic structure database (Shyu *et al.*, 2016), recurrence interval of the Milun fault is 66–67 yrs, due to its high slip rate (10.15 mm/yr) and small characteristic magnitude (M_w 6.4). According to a Poisson model adopted in

the TEM PSHA2015, its rupture probability for 50 yrs is 53% (green line in Fig. 4a). In addition to the time-independent Poisson model, Chan *et al.* (2017) have raised importance of time dependency for PSHA using the BPT model. We followed this assessment to evaluate rupture probability of the Milun fault. Considering recurrence interval of 67 yrs (according to Shyu *et al.*, 2016) and aperiodicity value of 0.5 (suggested by Chan *et al.*, 2017), the rupture probability on the Milun fault within 50 yrs can be expressed as a function of elapse time since last rupture (blue lines in Fig. 4a). Assuming elapse time of 67 yrs (last rupture during the 1951 Longitudinal Valley earthquake sequence (Yen *et al.*, 2018), the rupture probability in the coming 50 yrs is 80%. This model suggests significant high-seismic hazard from this fault, which can be associated with its rupture during the 2018 Hualien sequence.

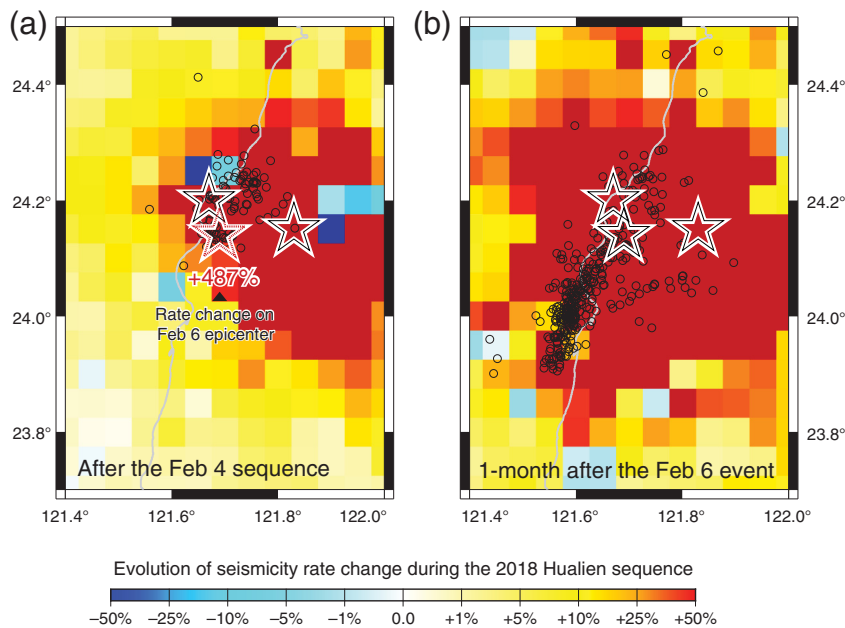
Although the TEM PSHA2015 model well forecasts the 2018 rupture on the Milun fault, the Hualien sequence has raised some disadvantages of this model. This assessment assumes seismogenic structures fully rupture only during earthquake events with maximum magnitude, i.e., partial rupture is not addressed. In addition, these seismogenic structures are



▲ **Figure 3.** The Molchan diagram used for investigating the correlation between forecasting models and seismicity with (a) $M_w \geq 4.0$ and (b) $M_w \geq 6.0$. Blue and green circles represent the results for the models using TEM PSHA2015 and the smoothing approach, respectively. Gray circles represent the 99% significance level determined by 603 forecasting events.



▲ **Figure 4.** Rupture probability for (a) the Milun fault and (b) the Longitudinal Valley fault as a function of time elapsed since last event based on the Brownian passage time (BPT) model (blue lines) and Poisson distribution (green lines). The rupture recurrence intervals of these faults are 67 and 189 yrs, respectively (Shyu *et al.*, 2016). The aperiodicity value (α) of 0.5 is assumed for the BPT model. Although both of the Milun and Longitudinal Valley faults ruptured in 1951 (time elapse of last event is 67 yrs), their rupture probabilities in the coming future are different due to different rupture recurrence intervals.



▲ Figure 5. Forecasted seismicity rates (a) immediately after the two 4 February events and (b) one month after the 6 February event and distribution of the Hualien sequence. The earthquakes take place during 4 and 23 February are denoted as black circles.

independent of one another; that is, neither multiple structure rupture nor earthquake triggering is expected. The 6 February M_w 6.3 event initiates on an unknown structure and continues rupture on the Milun fault in a single event, suggesting rupture on multiple structures (Lee *et al.*, 2018). In addition, considering its maximum magnitude of 6.4, the Milun fault ruptures only partially during this event (Lee *et al.*, 2018), which mismatches the model assumption. Such assumptions might mislead hazard potential in the fault system.

MODEL PERFORMANCE IN SHORT-TERM SEISMICITY EVOLUTION

Traditional PSHAs, including the TEM PSHA2015, assume that earthquakes are independent of one another (Merz and Cornell, 1973, and references therein). Such assumption, however, has been questioned, because previous shocks could trigger a subsequent earthquake sequence (Harris, 1998, and

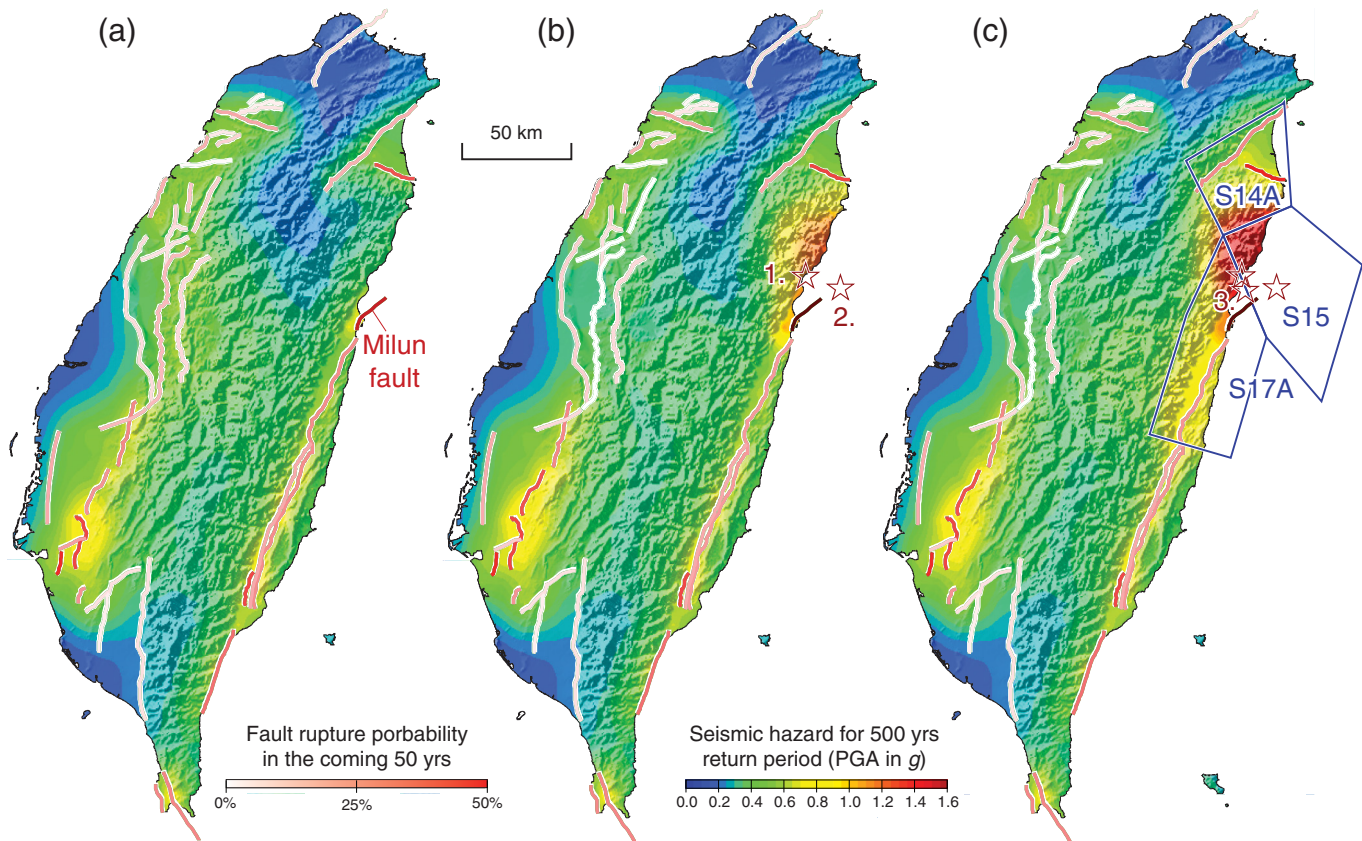
references therein). The 2018 Hualien sequence further confirmed this ambiguity, because the M_w 6.3 earthquake resulted in larger damages than damages by its foreshocks.

Because the current version of the TEM model follows the time-independent Poisson procedure, it is difficult to forecast seismicity evolution in an earthquake sequence. Alternatively, Chan *et al.* (2017) have proposed a time-dependent PSHA by implementing the rate-and-state friction model (Dieterich, 1994). This approach incorporates Coulomb stress changes of previous events resolved on each seismogenic source and quantifies their impacts into seismicity rate evolution. Following this approach, we evaluated rate evolution due to the three large earthquakes in the Hualien sequence (red stars in Fig. 1) using the Coulomb 3.4 code (Toda *et al.*, 2011). After occurrence of the two 4 February earthquakes, our model shows significant seismicity rate increase in their vicinity, including in the epicenter of the subsequent M_w 6.3 earthquake (dashed star in Fig. 5a). Additionally, these two events increased Coulomb stress for 0.3 bars on the Milun fault (Table 2), leading to the assumption that this triggered the M_w 6.3 event. After the M_w 6.3 earthquake, the model suggests seismicity rate enhanced further south, consistent with spatial distribution of consequent seismicity (Fig. 5b). This earthquake also promotes stress of 0.59 bars on the Milun fault and elevates seismic hazard level in its vicinity.

Based on the stress evolution model (shown in Fig. 5), we further quantified corresponding seismic hazard by assessing probabilistic seismic hazard at several time snapshots (Fig. 6). We first proposed a time-independent hazard map (Fig. 6a) as the basis of our seismic hazard model. It is identical to the hazard map of the TEM PSHA2015 (Wang, Chan, *et al.*, 2016), because they share identical parameters for seismogenic sources. Figure 6b,c shows results from our renewal models at different time snapshots. After occurrence of the two 4 February earthquakes, seismic hazard is elevated in their vicinity, which can be associated with higher expected rates on the shallow-background areas S14A, S15, and S17A (Table 1). In addition to the high rate in the shallow-background area S17A, the

Seismogenic Source	4 February M_w 4.9	4 February M_w 6.1	6 February M_w 6.3
Northern Ilan structure	0.00	+0.03	+0.12
Southern Ilan structure	0.00	+0.03	+0.09
Milun fault	0.00	+0.30	+0.59
Longitudinal Valley fault	0.00	0.00	+0.02

Epicenters of the three events and alignments of the four seismogenic structure sources are denoted in Figure 1.



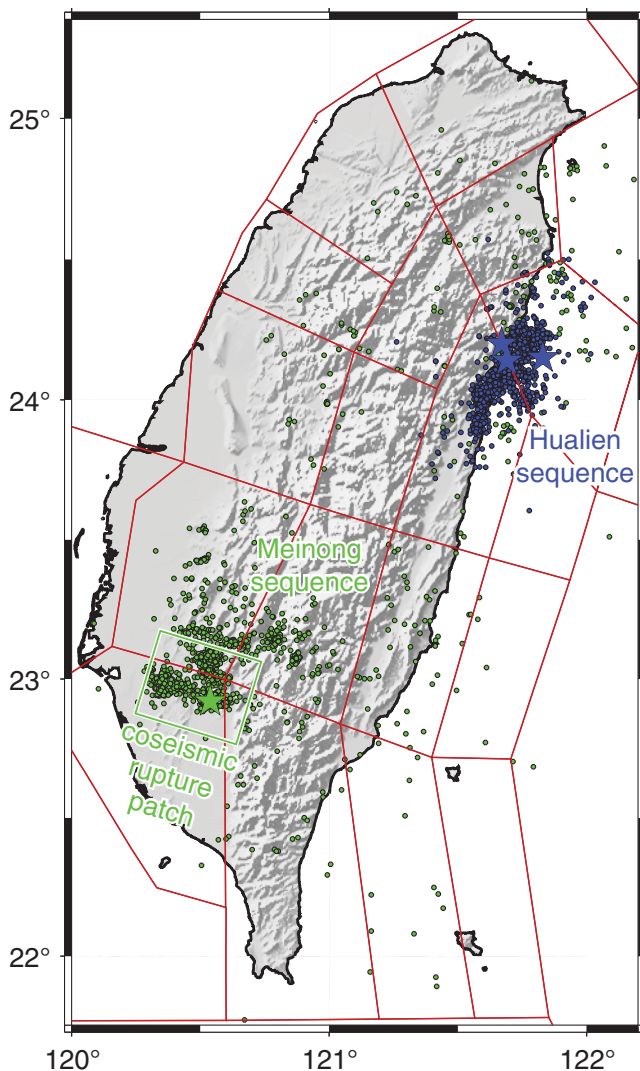
▲ **Figure 6.** (a) Time-independent and (b) time-dependent probabilistic seismic hazards immediately after the two 4 February events and (c) one month after the 6 February event. Stars 1–3 denote 4 February M_w 4.9, 4 February M_w 6.1, and 6 February M_w 6.3 earthquakes, respectively. The implemented earthquakes for short-term rate evolution for each time snapshot are denoted as stars. Rupture probability of each seismogenic structure source in the coming 50 yrs is presented in colors of white–red. The shallow-background areas S14A, S15, and S17A are denoted as blue polygon. The rupture probability for each seismogenic structure source is colored considering recurrence interval on each source, the Poisson (sources without last rupture time) or BPT (sources with last rupture time) models, and rate-and-state friction law.

high-rupture probability of the Milun fault (Fig. 6b) implies occurrence of the M 6.3 earthquake two days later. After the 6 February earthquake, this earthquake enhances seismicity on the neighboring shallow-background area sources (Table 1), resulting in significant higher hazard in northeast Taiwan (Fig. 6c), consistent with the earthquake burst afterward (Fig. 1). Because of Coulomb stress increase during this sequence (Table 2), the rupture probability on the Milun fault remains high (assuming this fault does not rupture entirely in the Hualien sequence). The hazard along the Longitudinal Valley becomes higher, which can be associated with increased Coulomb stress change in the area source of S17A (blue polygon in Fig. 6c), rather than contribution from individual seismogenic structure sources (shown in Table 2).

SUGGESTIONS FOR NEXT GENERATION OF TAIWAN EARTHQUAKE MODEL

In this study, we validated performance of the TEM PSHA2015 during the 2018 Hualien sequence and compared

with other PSHA approaches. The forecasting models by the shallow-background area source (Fig. 2a) and the smoothing models (Fig. 2b) show spatial heterogeneous patterns in detail, because area source averages the seismicity rate in each defined area, whereas smoothing models assume highest rate at each epicenter and decay with distance. However, Molchan diagrams confirm that both models obtain good forecasting ability (Fig. 3). It is worth mentioning that defining geometry of shallow-background area source could be difficult in a region with complex tectonic setting. Such disadvantage has been exposed in the cases of the Hualien and the 2016 Meinong sequences (Lee *et al.*, 2017), because each of them covers more than two shallow-background area sources (Fig. 7). Such phenomenon departs from the assumption of a traditional PSHA; that is, that one earthquake should take place in a single source and that each source is independent of one another. A smoothing model might be a solution for this ambiguity, because it does not require definition of area geometry. Thus, we suggest incorporating a smoothing model in the next generation of PSHA for Taiwan as a branch of logic tree.



▲ **Figure 7.** Distribution of seismicity after the 2016 Meinong (during 5–10 February 2016, green circles) and 2018 Hualien (during 4–23 February 2018, blue circles) earthquakes. The Meinong mainshock is denoted as the green star and the three largest events of the Hualien sequence are denoted as blue stars. The rupture zone of the Meinong earthquake derived from Shiann-Jong Lee (see [Data and Resources](#)) is denoted as green rectangle. Because all of the events taking place after the two earthquakes are shown, some far away from the mainshocks might not be regarded as their aftershocks.

In addition to shallow-background area sources, we also examined another category of seismogenic sources in the TEM PSHA2015 model, seismogenic structure source, through evaluating rupture probability of the Milun fault, which ruptures in the Hualien sequence. The Poisson model implemented in the TEM PSHA2015 forecasts its rupture probability of 53%, and the BPT model forecasts 80% before occurrence of this sequence (Fig. 4a). Because the BPT model considers memory time elapse of last rupture, which may provide better constraint on rupture forecasting, we suggest imple-

menting this model, especially for the seismogenic structure sources with records of their last ruptures.

In the Hualien sequence, a larger event follows a series of foreshocks and results in damage and fatality; hence the importance of short-term seismic hazard assessment has been raised. The current TEM model does not obtain this capability and the time-dependent PSHA proposed by [Chan et al. \(2017\)](#) could fill this gap. For the application to the Hualien sequence, we confirmed the feasibility of the [Chan et al. \(2017\)](#) approach, which well forecasts occurrence of the 6 February M_w 6.3 event, rupture on the Milun fault, and occurrence of subsequent earthquakes. This approach might shed light on rapid evaluations of consequent hazards, beneficial to decision makers and public officials. This approach is based on the rate-and-state friction model, which assumes that duration of seismicity rate change is proportional to aftershock duration ([Dieterich, 1994](#)). Most aftershock sequences in Taiwan have relatively short durations (between approximately 100 days to several years, [Chan and Wu, 2012](#)), resulting in rate perturbation only in a short period. Thus, its impact in a long assessing period, such as in 50 yrs (period of interest for standard PSHAs), becomes trivial. Such limitation of this model has also been raised by [Chan et al. \(2017\)](#), who compared seismic hazard maps based on different assessing periods and concluded the short-term factor of this approach becomes insignificant when assessing periods that are longer (fig. 6b–d of [Chan et al., 2017](#)).

DATA AND RESOURCES

The source parameters of our seismic hazard model are from the Taiwan earthquake model (TEM). The relocated earthquake parameters of the 2018 Hualien sequence were derived from Yen-Lin Chen (https://www.dropbox.com/s/q4n8y6ivqpv5ioy/CWB_aftershocks.zip?dl=0&fb=1&fb_action_ids=1452152718241534&fb_action_types=groups.post, last accessed April 2018). The detailed slip dislocation model of the 6 February 2016, Meinong M_w 6.5 earthquake was derived from Shiann-Jong Lee (http://tec.earth.sinica.edu.tw/new_web/upload/news/Conference/20160206meilongEQ/2016-02-06-slip.txt, last accessed July 2018). Our seismic hazard analysis is calculated using the OpenQuake Engine 3.1.0 (<https://storage.globalquakemodel.org/openquake/about/>, last accessed June 2018). ✉

ACKNOWLEDGMENTS

This research is supported by the National Research Foundation Singapore and the Singapore Ministry of Education under the Research Centres of Excellence initiative.

REFERENCES

- Chan, C. H., and Y. M. Wu (2012). A seismicity burst following the 2010 M 6.4 Jiashian earthquake—Implications for short-term seismic hazards in southern Taiwan, *J. Asian Earth Sci.* **59**, 231–239.
- Chan, C. H., Y. Wang, Y. J. Wang, and Y. T. Lee (2017). Seismic-hazard assessment over time: Modeling earthquakes in Taiwan, *Bull. Seismol. Soc. Am.* **107**, no. 5, 2342–2352, doi: [10.1785/0120160278](https://doi.org/10.1785/0120160278).

- Chan, C. H., Y. M. Wu, and J. P. Wang (2012). Earthquake forecasting using the rate-and-state friction model and a smoothing Kernel: Application to Taiwan, *Nat. Hazards Earth Syst. Sci.* **12**, no. 10, 3045–3057.
- Cheng, C.-T., P.-S. Hsieh, P.-S. Lin, Y.-T. Yen, and C.-H. Chan (2015). Probability seismic hazard mapping of Taiwan, in *Encyclopedia of Earthquake Engineering*, M. Beer, I. A. Kougioumtzoglou, E. Patelli, and I. S.-K. Au (Editors), Springer, Berlin, Germany, doi: [10.1007/978-3-642-36197-5_100-1](https://doi.org/10.1007/978-3-642-36197-5_100-1).
- Cornell, C. A. (1968). Engineering seismic risk analysis, *Bull. Seismol. Soc. Am.* **58**, 1583–1606.
- Dieterich, J. (1994). A constitutive law for rate of earthquake production and its application to earthquake clustering, *J. Geophys. Res.* **99**, 2601–2618.
- Ellsworth, W. L., M. V. Matthews, R. M. Nadeau, S. P. Nishenko, P. A. Reasenber, and R. W. Simpson (1999). A physically based earthquake recurrence model for estimation of long-term earthquake probabilities, *U.S. Geol. Surv. Open-File Rept.* 99-522, 1–12.
- Gutenberg, B., and C. F. Richter (1944). Frequency of earthquakes in California, *Bull. Seismol. Soc. Am.* **34**, no. 4, 185–188.
- Harris, R. A. (1998). Introduction to special section, stress triggers, stress shadows, and implications for seismic hazard, *J. Geophys. Res.* **103**, 24,347–24,358.
- Lee, S. J., T. C. Lin, T. Y. Liu, and T. P. Wong (2018) Fault-to-fault jumping rupture of the 2018 M_w 6.4 Hualien earthquake in eastern Taiwan, *Seismol. Res. Lett.* doi: [10.1785/0220180182](https://doi.org/10.1785/0220180182).
- Lee, Y. T., Y. J. Wang, C. H. Chan, and K. F. Ma (2017). The 2016 Meinong earthquake to TEM PSHA2015, *Terr. Atmos. Ocean. Sci.* **28**, 703–713, doi: [10.3319/TAO.2016.12.28.02](https://doi.org/10.3319/TAO.2016.12.28.02).
- Merz, H. A., and C. A. Cornell (1973). Seismic risk analysis based on a quadratic magnitude-frequency law, *Bull. Seismol. Soc. Am.* **63**, 1999–2006.
- Molchan, G. M. (1990). Strategies in strong earthquake prediction, *Phys. Earth Planet. In.* **61**, 84–98.
- Shyu, J. B. H., Y. R. Chuang, Y. L. Chen, Y. R. Lee, and C. T. Cheng (2016). A new on-land seismogenic structure source database from the Taiwan earthquake model (TEM) project for seismic hazard analysis of Taiwan, *Terr. Atmos. Ocean. Sci.* **27**, no. 3, 311–323.
- Toda, S., R. S. Stein, V. Sevilgen, and J. Lin (2011). Coulomb 3.3 graphic-rich deformation and stress-change software for earthquake, tectonic, and volcano research and teaching—user guide, *U.S. Geol. Surv. Open-File Rept.* 2011-1060, 63 pp., Earthquake Science Center, Menlo Park Science Center, Menlo Park, California.
- Wang, Y. J., C. H. Chan, Y. T. Lee, K. F. Ma, J. B. ShyuH, and R. J. Rau (2016). Probabilistic seismic hazard assessments for Taiwan, *Terr. Atmos. Ocean. Sci.* **27**, no. 3, 325–340.
- Wang, Y. J., Y. T. Lee, C. H. Chan, and K. F. Ma (2016). An investigation of the reliability of the Taiwan earthquake model PSHA2015, *Seismol. Res. Lett.* **88**, no. 2A, doi: [10.1785/0220160085](https://doi.org/10.1785/0220160085).
- Woo, G. (1996). Kernel estimation methods for seismic hazard area source modeling, *Bull. Seismol. Soc. Am.* **86**, 353–362.
- Wu, Y. M., M. Mittal, T. C. Huang, B. M. Yang, J. C. Jan, and S. K. Chen (2018) Performance of a low-cost earthquake early warning system (P-Alert) and shake map production during the 2018 M_w 6.4 Hualien, Taiwan, earthquake, *Seismol. Res. Lett.* doi: [10.1785/0220180170](https://doi.org/10.1785/0220180170).
- Yen, J. Y., C. H. Lu, R. J. Dorsey, H. Kuo-Chen, C. P. Chang, C. C. Wang, R. Y. Chuang, Y. T. Kuo, C. Y. Chiu, Y. H. Chang, *et al.* (2018) Insights into seismogenic deformation during the 2018 Hualien (Taiwan) earthquake sequence from InSAR, GPS, and modeling, *Seismol. Res. Lett.* doi: [10.1785/0220180228](https://doi.org/10.1785/0220180228).
- Zechar, J. D., and T. H. Jordan (2008). Testing alarm-based earthquake predictions, *Geophys. J. Int.* **172**, no. 2, 715–724.

Chung-Han Chan
Earth Observatory of Singapore
Nanyang Technological University
N2-01a-14, 50 Nanyang Avenue
Singapore 639798
hantijun@googlemail.com

Kuo-Fong Ma¹
Ya-Ting Lee¹
Earthquake-Disaster & Risk Evaluation and Management
(E-DREaM) Center
National Central University
No. 300, Zhongda Road, Zhongli District
Taoyuan City 32001, Taiwan

Yu-Ju Wang
Department of Nuclear Backend Management
Taiwan Power Company
No. 242, Section 3, Roosevelt Road, Zhongzheng District
Taipei City 10016, Taiwan

Published Online 31 October 2018

¹ Also at Department of Earth Sciences, National Central University, Taiwan.